Applicability of time-average moiré techniques for chaotic oscillations

Minvydas Ragulskis,[1] Miguel A. F. Sanjuan,[2] and Loreta Saunoriene[1]

[1]*Department of Mathematical Research in Systems, Kaunas University of Technology, Studentu 50-222, 51638, Kaunas, Lithuania*
[2]*Nonlinear Dynamics and Chaos Group, Departamento de Fisica, Universidad Rey Juan Carlos, Mostoles, 28933,*

Madrid, Spain

Applicability of time-average moiré techniques for chaotic oscillations is analyzed in this paper. Envelope function characterizing the rate of convergence of time-averaged color intensity is derived. A study of the relationship among Lyapunov exponents and gray scale color intensity provides insight into the process of chaotic contrast modulation and confirms that chaotic oscillations do not produce time-average moiré fringes.

I. INTRODUCTION

Regular optical patterns can be exploited for characterization of spatially and periodically forced nonlinear systems [1]. Moiré is a classical experimental technique exploiting optical patterns with many applications [2,3] in different fields of science and engineering. This technique is based on the analysis of visual patterns produced by the superposition of two regular gratings that interfere geometrically. Examples of such gratings are equispaced parallel lines, concentric circles, and radial lines [4–6]. The gratings can be superposed by double exposure photography, by reflection, by shadowing, or even by direct contact [7–9]. Moreover, moiré patterns are used to measure displacements, rotations, curvature, and strain through the viewed area.

Time-averaging optical techniques possess a definite advantage over double exposure techniques in the sense that periodic or even transient dynamical processes can be investigated directly [10]. Time-average geometric moiré exploits the grating formed on the surface of an elastic oscillating structure. Time-averaged fringes are produced when the carrier moiré grating is contrast modulated by the function dependent on the type of the object motion. Dynamic displacements can be estimated from the time-averaged fringes, whereas the fringe order no longer represents the displacement by an integer number of pitches. Moreover, the intensity of the time-averaged moiré pattern is governed by relationships comprised of a zero order Bessel function of the first kind [2,3,11,12].

It is well known that nonlinear systems can exhibit periodic, quasiperiodic, and even chaotic responses under periodic forcing [13–15]. Therefore, it is important to understand what time-averaged image would be produced if a moiré grating is formed on the surface of a chaotically oscillating elastic structure.

The influence that classical dynamics has on interference patterns in coherence experiments is discussed in [16]. A time-integrated probability current is calculated through an absorbing screen, and furthermore it is shown how interference fringes in the probability current generically disappear in the case of a chaotic system.

The object of this paper is to analyze how the time-average pattern of fringes generated by optical experimental techniques can be used to determine the chaotic dynamics of certain mechanical structures. The ability to interpret such time-averaged moiré images would help to improve the uncertainty of the inverse problem and to distinguish malfunctions of the optical setup and also physical reasons causing specific optical effects.

II. ILLUSTRATIVE EXAMPLE

Bending vibrations play a crucial role in the functionality of different micromechanical systems such as cantilevers, micromirrors, etc. [14]. A typical example is a centrally clamped rotating circular disk, where bending vibrations can affect the operation of hard disk drives [18,19]. It is natural to expect that those vibrations can be quasiperiodic or even chaotic. We follow a universal approach to the investigation of the dynamics in generalized models proposed in [20] when a single generalized model can describe a class of systems, which share a similar structure.

The construction of digital time-averaged reflection moiré images for harmonically oscillating structures is presented in detail in [21]. Finite element computational techniques are used to build the model of a centrally clamped disk. A finite element mesh and the tenth eigenmode of a centrally clamped disk are shown in Fig. 1(a). The mesh in the state of equilibrium is gray and deflected according to the eigenmode, which is black. It is assumed that an ideal mirror film covers the surface of the disk and a semisilvered mirror is used in order to assure that the moiré grating and the photographic plate would not overlap each other.

It is assumed that the vibration energy of the analyzed disk is concentrated in just one mode (the tenth mode). The double exposure reflection moiré image [Fig. 1(b)] corresponds to a special stroboscopic analysis technique over a harmonically oscillating disk when the images of the disk in the state of equilibrium and in the state of maximum deflection are overlapped. The time-average reflection moiré image [Fig. 1(c)] is constructed for a harmonically oscillating disk; calculations are performed over one period of the oscillations. A produced digital image demonstrates a well-defined pattern of fringes, which can be effectively applied for the reconstruction of dynamical deflections [21].

In order to investigate the applicability of time-average moiré techniques for chaotic oscillations, we consider a nonlinear periodically driven damped pendulum, which is a
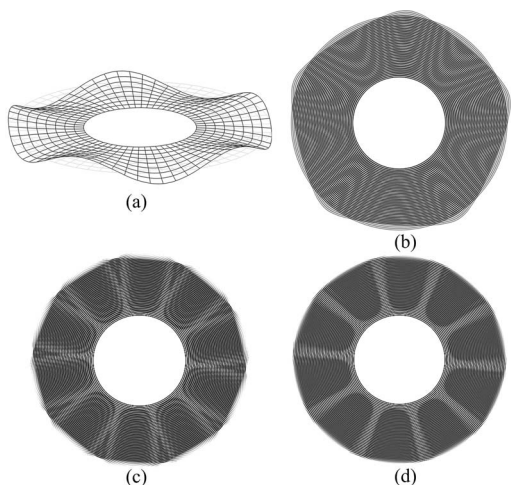
FIG. 1. Applicability of moiré techniques for determination of chaotic oscillations: (a) FEM (finite element method) model of the centrally clamped disk: light gray lines—disk in the state of equilibrium; dark lines—disk deflected according to the tenth eigenform; (b) double exposure reflection moiré image of the disk; (c) time-average reflection moiré for harmonic oscillations; (d) time-average reflection moiré for chaotic oscillations.

paradigm in the study of nonlinear dynamics. A dimensionless time evolution equation of such a pendulum reads [13]

$$\frac{d^2\theta}{dt^2} = -\sin\theta - b\frac{d\theta}{dt} + F\cos(\omega t), \qquad (1)$$

where b is the damping coefficient, F is the external forcing amplitude, and ω is the frequency. The driven damped pendulum with $\omega=23$, $b=1.0$, and $F=2.048$ yields chaotic behavior following a period-doubling sequence of bifurcations [Fig. 2]. Phase trajectories in the insets of Fig. 3 are plotted in frames $(\theta;\dot{\theta})$ at the following values of b: (a) $b=1.04$, (b) $b=1.025$, (c) $b=1.01$, (d) $b=1.0055$, (e) $b=1.003$, and (f) b
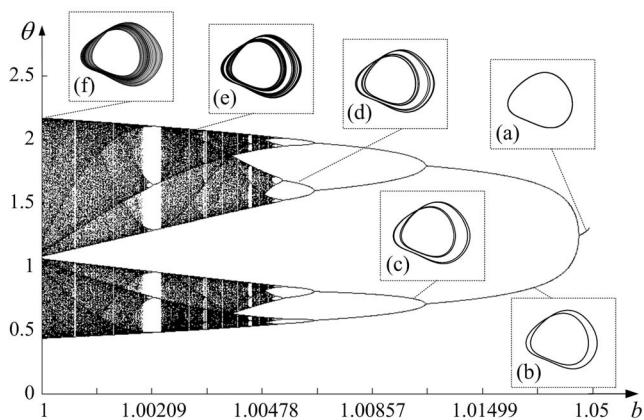

FIG. 2. Bifurcation diagram for the driven damped nonlinear pendulum with parameter values $\omega=2/3$, $F=2.048$, with respect to the variation of the damping coefficient b. The insets show phase space diagrams with orbits corresponding to specific values of the parameters.
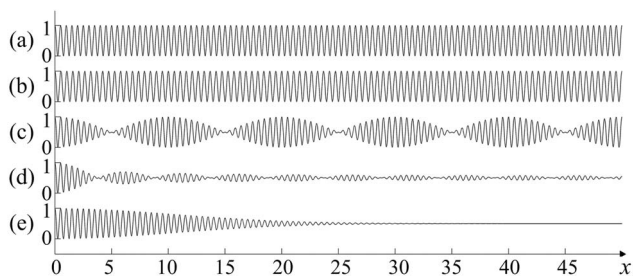

FIG. 3. Disappearance of fringes caused by chaotic oscillations at $u(x)=kx$: (a) $I_0(x)$—one-dimensional system in the state of equilibrium; (b) $I_1(x)$—deformed state; (c) $I_d(x)$—double exposure of $I_0(x)$ and $I_1(x)$; (d) $I_t(x)$—time-averaged fringes produced by harmonic oscillations; (e) $I_\theta(x)$—no time-averaged fringes are formed when oscillations are chaotic (at $\lambda=0.5$; $k=0.05$; $\sigma=0.15$).

$=1.0002$. Parameter b is varied following the rule $b_i=1.05-\frac{0.05}{\ln 201}\ln(1+\frac{1000-i+1}{5})$; $i=1,\dots,1001$, which helps to expand the cascade of period-doubling bifurcations.

The time-average reflection moiré image for chaotic oscillations [Fig. 1(d)] is constructed under the assumption that the modal deflection of the disk varies according to the amplitude of the time process of a driven nonlinear pendulum at $b=1.002$ [variant (f) in Fig. 2]. A long exposure time is used to construct Fig. 1(d); disk deflections at 500 discrete time moments of the evolution of θ defined by Eq. (1) are evaluated, which corresponds to 20 periods of the external perturbation. This is a large computational problem keeping in mind that finite element techniques are used to reconstruct individual pixel gray scale color intensities at appropriate discrete time moments, and time-averaging techniques are applied afterwards to construct the time-averaged image [11].

No definite pattern of fringes is present in the time-average moiré image constructed for chaotic oscillations [Fig. 1(d)], though the original moiré grating is clear in the regions where the magnitude of dynamic deflections from the state of equilibrium is infinitesimal. As mentioned earlier, the results presented in Fig. 1(d) are constructed under the assumption that the vibration energy is concentrated in the tenth mode. If the vibration energy would travel from one mode to another (what is a rather common situation in nonlinear systems [22,23]) the digital image would be blurred in the whole area of the disk (except the zone around the fixed internal radius) and no modal shapes could be reconstructed from time-averaged images. In order to investigate the physical reasons causing fringe patterns getting blurred, we concentrate on the analysis of one-dimensional moiré systems.

III. ONE-DIMENSIONAL SYSTEMS

Moiré grating on the surface of a one-dimensional structure in the state of equilibrium can be defined as a harmonic variation of gray scale color in the range between 0 (representing black color) and 1 (representing white color) defined by (Ref. [11])

$$I_0(x) = \cos^2\left(\frac{\pi}{\lambda}x\right), \tag{2}$$

where I_0 is the gray scale color intensity in the state of equilibrium, x is the longitudinal coordinate, and λ is the pitch of the grating. The gray scale color intensity is a continuous function and its linewidth is 50% of the pitch.

The gray scale color intensity of the one-dimensional structure in a deformed state I_1 can be described as

$$I_1(x) = \cos^2\left(\frac{\pi}{\lambda}[x - u(x)]\right), \tag{3}$$

where $u(x)$ is the displacement from the state of equilibrium.

Superposition of the grating in the state of equilibrium and in the deformed state produces a pattern of double exposure moiré fringes [11] given by

$$I_d(x) = \frac{1}{2}[I_0(x) + I_1(x)]$$

$$= \frac{1}{2} + \frac{1}{2}\cos\left[\frac{2\pi}{\lambda}\left(1 - \frac{u(x)}{2x}\right)x\right]\cos\left(\frac{\pi}{\lambda}u(x)\right). \tag{4}$$

The centers of the generated fringes are located at such values of x, where the branches of the envelope function of the beatings $\frac{1}{2} \pm \frac{1}{2}\cos\left[\frac{\pi}{\lambda}u(x)\right]$ intersect. The relationship among time-averaged fringes of order n, the pitch of the grating, and the displacement can be derived from the condition $I_d(x) = 0.5$, giving

$$u(x) = \lambda\left(n - \frac{1}{2}\right). \tag{5}$$

When time-averaging techniques are applied for the analysis of a harmonically oscillating elastic one-dimensional structure, the carrier fringes are contrast modulated and the intensity of the time-average geometric moiré image I_t is described as [12]

$$I_t(x) = \lim_{T\to\infty}\frac{1}{T}\int_0^T \cos^2\left(\frac{\pi}{\lambda}[x - u(x)\sin(\omega t - \varphi)]\right)dt$$

$$= \frac{1}{2} + \frac{1}{2}\cos\left(\frac{2\pi}{\lambda}x\right)J_0\left(\frac{2\pi}{\lambda}u(x)\right), \tag{6}$$

where T is the time of exposure, ω and φ are the angular frequency and the phase of harmonic oscillations around the state of equilibrium, J_0 is the zero order Bessel function of the first kind, and $u(x)$ now defines the amplitude of dynamic displacement. The centers of the time-average fringes are located at such values of x where the branches of the envelope function $\frac{1}{2} \pm \frac{1}{2}J_0\left[\frac{2\pi}{\lambda}u(x)\right]$ intersect, giving

$$u(x) = \frac{\lambda}{2\pi}r_n, \tag{7}$$

where r_n is the nth root of J_0. It should be noted that neither the frequency nor the phase can be reconstructed from the pattern of time-averaged fringes.

If the oscillation of the analyzed one-dimensional system is not harmonic, the intensity of the time-averaged gray scale intensity is

$$I_\theta(x) = \lim_{T\to\infty}\frac{1}{T}\int_0^T \cos^2\left(\frac{\pi}{\lambda}[x - u(x)\theta(t)]\right)dt, \tag{8}$$

where $\theta(t)$ is a function determining the variation of the displacements $u(x)$ in time. If $\theta(t)$ is a Gaussian normal ergodic process, it can be approximated by a discrete scalar series of normally distributed numbers with zero mean and σ^2 variance

$$\theta_i \sim N(0, \sigma^2), \quad i = 1, 2, \dots. \tag{9}$$

Initial moments of such random variables are

$$E\theta^{2k-1} \equiv 0, \quad k = 1, 2, 3, \dots,$$

$$E\theta^{2k} \equiv 1 \times 3 \times \cdots \times (2k-1)\sigma^{2k} = (2k-1)!!\,\sigma^{2k},$$

$$k = 1, 2, 3, \dots. \tag{10}$$

Then it is possible to use the following approximations:

$$\lim_{T\to\infty}\frac{1}{T}\int_0^T \cos[au(x)\theta(t)]dt$$

$$= \lim_{m\to\infty}\frac{1}{m}\sum_{i=1}^m \cos[au(x)\theta_i]$$

$$= \lim_{m\to\infty}\frac{1}{m}\sum_{i=1}^m \sum_{k=0}^{+\infty}\frac{(-1)^k[au(x)\theta_i]^{2k}}{(2k)!}$$

$$= \sum_{k=0}^{+\infty}\frac{(-1)^k[au(x)]^{2k}}{(2k)!}\lim_{m\to\infty}\sum_{i=1}^m\frac{(\theta_i)^{2k}}{m}$$

$$= \sum_{k=0}^{+\infty}\frac{(-1)^k[au(x)]^{2k}}{(2k)!}(2k-1)!!\,\sigma^{2k}$$

$$= \sum_{k=0}^{+\infty}\frac{(-1)^k[au(x)\sigma]^{2k}}{(2k)!!} = \sum_{k=0}^{+\infty}\frac{(-1)^k[au(x)\sigma]^{2k}}{2^k k!}$$

$$= \sum_{k=0}^{+\infty}\frac{(-1)^k}{k!}\left[\frac{1}{2}[au(x)\sigma]^2\right]^k = \exp\left[-\frac{1}{2}[au(x)\sigma]^2\right], \tag{11}$$

and

$$\lim_{T\to\infty}\frac{1}{T}\int_0^T \sin[au(x)\theta(t)]dt$$

$$= \lim_{m\to\infty}\frac{1}{m}\sum_{i=1}^m \sin[au(x)\theta_i]$$

$$= \lim_{m\to\infty}\frac{1}{m}\sum_{i=1}^m \sum_{k=0}^{+\infty}\frac{(-1)^k[au(x)\theta_i]^{2k+1}}{(2k+1)!}$$

$$= \sum_{k=0}^{+\infty}\frac{(-1)^k[au(x)]^{2k+1}}{(2k+1)!}\lim_{m\to\infty}\sum_{i=1}^m\frac{(\theta_i)^{2k+1}}{m} = 0, \tag{12}$$
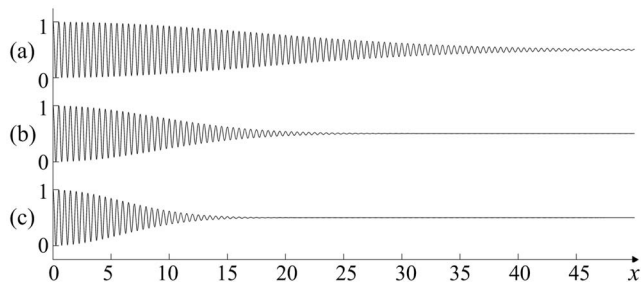
FIG. 4. Convergence of $I_\theta(x)$ to 0.5 at different values of σ at $u(x)=kx$, $\lambda=0.5$, $k=0.05$: (a) $\sigma=0.09$; (b) $\sigma=0.18$; (c) $\sigma=0.27$.

where a is a constant. This leads to the following result:

$$I_\theta(x) = \frac{1}{2} + \frac{1}{2}\cos\left(\frac{2\pi}{\lambda}x\right)\lim_{T\to\infty}\frac{1}{T}\int_0^T \cos\left(\frac{2\pi}{\lambda}u(x)\theta(t)\right)dt$$

$$- \frac{1}{2}\sin\left(\frac{2\pi}{\lambda}x\right)\lim_{T\to\infty}\frac{1}{T}\int_0^T \sin\left(\frac{2\pi}{\lambda}u(x)\theta(t)\right)dt$$

$$= \frac{1}{2} + \frac{1}{2}\cos\left(\frac{2\pi}{\lambda}x\right)\exp\left[-\frac{1}{2}\left(\frac{2\pi}{\lambda}u(x)\sigma\right)^2\right]. \quad (13)$$

Finally, the envelope function of the contrast modulated carrier fringes takes the following form:

$$E_\theta(x) = \frac{1}{2} \pm \frac{1}{2}\exp\left[-\frac{1}{2}\left(\frac{2\pi}{\lambda}u(x)\sigma\right)^2\right]. \quad (14)$$

Equation (14) shows an interesting feature. Time-averaged gray scale color intensity converges exponentially to the value of 0.5 at increasing dynamic displacements. Moreover, no time-averaged fringes are formed at all. The higher is the variance, the faster is the convergence. These effects are illustrated in Figs. 3 and 4.

IV. RELATIONSHIP BETWEEN THE LARGEST LYAPUNOV EXPONENT AND TIME-AVERAGED GRAY SCALE INTENSITY

Lyapunov exponents provide a quantitative measure of the degree of chaoticity for a trajectory in the theory of both Hamiltonian and dissipative dynamical systems. Therefore there exists a definite interest to observe possible relationships among the largest Lyapunov exponent of the time function $\theta(t)$ and the gray scale color intensity in time-averaged moiré images.

We focus on the same nonlinear periodically driven damped pendulum used to illustrate the blurred pattern of fringes formed by bending oscillations of the disk (Eq. (1)). Local Lyapunov coefficients are calculated at specified values of the damping coefficient b. The Jacobian of Eq. (1) is

$$J = \begin{pmatrix} 0 & 1 & 0 \\ -\cos\theta & -b & -\omega F\sin(\omega t) \\ 0 & 0 & 0 \end{pmatrix}.$$

Then, the calculation of the maximum, λ_1, and the minimum, λ_2, local Lyapunov exponents [17] is straightforward.
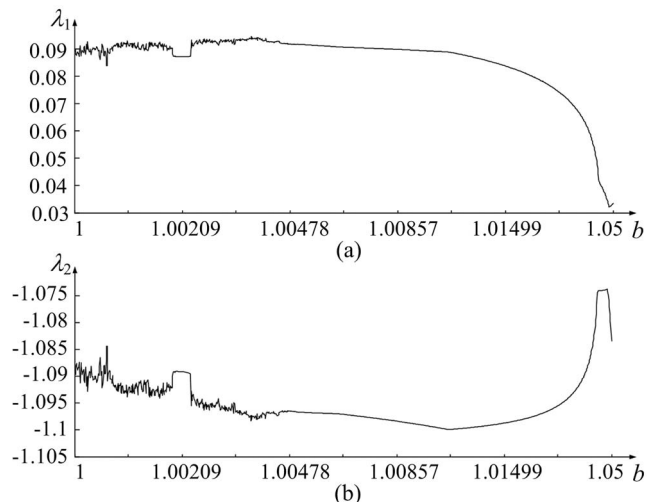

FIG. 5. The figure shows the variation of the Lyapunov exponents of the driven damped nonlinear pendulum as the damping coefficient b increases; $\omega=2/3$, $F=2.048$. (a) Maximum Lyapunov exponent. (b) Minimum Lyapunov exponent.

$$\lambda_1 = -\frac{b}{2} + \sqrt{\frac{b^2}{4} - \cos\theta},$$

$$\lambda_2 = -\frac{b}{2} - \sqrt{\frac{b^2}{4} - \cos\theta}. \quad (15)$$

Sufficiently long time evolutions of θ (after the transients seize down) are used in Eq. (15) to calculate averaged approximations of local Lyapunov exponents, which are shown in Fig. 5.

Table I shows Lyapunov exponents calculated at different values of b, which were used to visualize phase trajectories in Fig. 2. Now the one-dimensional Moiré system is analyzed again. It is assumed that the time function $\theta(t)$ in Eq. (8) is the time evolution of θ defined by Eq. (1). Naturally, only the steady state time evolution of θ is considered without the starting transients. Long time processes are used in order to eliminate the effect of the mismatch between the starting and finishing phases. Moreover, as the variation of b alters the geometrical shape of the attractor, the time process is linearly rescaled so that its mean is equal to 0 and its variance is equal to 1.

Time-averaged gray scale color intensities are presented in Fig. 6. It can be clearly seen that the range of time-averaged gray scale color intensities is located around 0.5 at higher magnitudes of maximum Lyapunov exponent. The higher the maximum Lyapunov exponent is, the faster the time-averaged image is blurred. The carrier fringes are still of course visible in the region where $u(x)$ is small.

It is clear that the dynamical variable of the nonlinear driven pendulum [Eq. (1)] does not have a Gaussian ergodic distribution when the dynamics is chaotic. Nevertheless, the effect of the disappearance of fringes observed when the chaotic dynamics is described by the dynamic variable of the pendulum is similar to the effect when the dynamic variable

TABLE I. Local averaged Lyapunov exponents of the driven damped nonlinear pendulum; $\omega=2/3$; $F=2.048$.

No.	λ_1	λ_2	$\lambda_1+\lambda_2$	b
(a)	0.03382465351905	−1.07382465351910	−1.04000000000005	1.0400
(b)	0.06747440395449	−1.09247440395691	−1.02500000000242	1.0250
(c)	0.08923170163203	−1.09923170163331	−1.01000000000128	1.0100
(d)	0.09132576753700	−1.09682576753777	−1.00550000000077	1.0055
(e)	0.09259723521378	−1.09559723521619	−1.00300000000241	1.0030
(f)	0.09269473920576	−1.09289473920214	−1.00020000000362	1.0002

is approximated by a Gaussian ergodic distribution. Therefore, it would be interesting to know if similar effects causing the fringes to disappear can be observed when the oscillations are, in general, not periodic (being quasiperiodic, chaotic, or stochastic with whatever distribution function).

The effect of the disappearance of fringes at nonharmonic oscillations can be explained by the following considerations. Harmonic oscillations produce a well-defined pattern of time-averaged fringes. In fact, it is enough to average over one full period of harmonic oscillations to produce this pattern. We assume that the amplitude of harmonic oscillations has changed to another discrete value after the first period of the oscillations. The frequency of the oscillations is not important as time averaging eliminates all information about the frequency [Eq. (6)]. Then, time averaging over the second full period of harmonic oscillations would produce a different pattern of fringes, which generally is not repetitive to the first pattern of fringes. Then, after the second period, the amplitude is changed again. If we continue such a process for a long time, time averaging would not produce time-average fringes and the image would get blurred at higher dynamic displacements.

If the dynamic variable is described by a stochastic distribution, the effect of image blurring is even faster compared with quasiperiodic or chaotic oscillations. Time-averaged
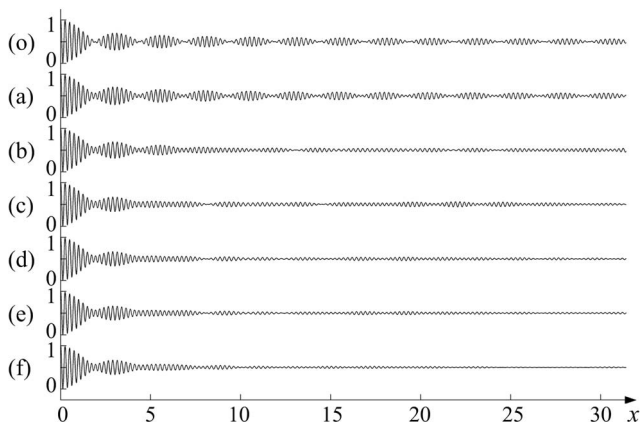

FIG. 6. Disappearance of fringes caused by chaotic oscillations: (o) time-averaged fringes produced by harmonic oscillations at $\theta=\sin(t)$, $\lambda_1=0$: (a) time-averaged gray scale intensities $I_\theta(x)$ at $\lambda=0.25$, $u=kx$, $k=0.05$, $\omega=2/3$, $F=2.048$, $b=1.04$, $\lambda_1=0.0338$; (b) $b=1.025$, $\lambda_1=0.0675$; (c) $b=1.01$, $\lambda_1=0.0892$; (d) $b=1.0055$, $\lambda_1=0.0913$; (e) $b=1.003$, $\lambda_1=0.0925$; and (f) $b=1.0002$, $\lambda_1=0.0926$.

color intensity converges to 0.5 at higher dynamic displacements (Gaussian distribution), while some undeveloped fringes can still be seen in Fig. 6 at lower values of λ_1. We have also analyzed stochastic oscillations with even distribution in a fixed interval and the results are similar to a Gaussian distribution—time-averaged intensity converges to 0.5 without any (even undeveloped) fringes.

Another important question is whether the malfunction of an optical setup can be distinguished from the optical effects caused by chaotic oscillations. And in the case that chaotic oscillations can be identified, what useful information one can obtain by looking at the time-averaged image.

Defocus, geometrical or physical defects of optical or mechanical elements, camera shake, and misalignment of optical components are main sources of problems associated with the malfunction of optical measurement systems. Though such defects usually cause uniform blurs throughout the image area, there exists a probability that only some part of the image could be blurred (caused, for example, by a stain on a lens). The optical system can be calibrated before the measurement, but even if some defects would occur during the measurement process, novel computational imaging techniques [24] could be exploited to enhance the view. Thus stationary images blurred by the optical system can be more or less successfully deblurred. But it is impossible to use computational image reconstruction techniques to enhance the fringes blurred by chaotic oscillations—the fringes simply do not form then. If one still would have doubts if the image blur is caused by chaotic oscillations or optical malfunctions, one should register a stationary image (for example, the image of the moiré grating used in time-averaging experiments). Possible blurs caused by the optical system should clarify the dissociation then.

Thus one can be sure that the analyzed system was performing nonharmonic oscillations if moiré grating can be clearly visible at least in some parts of the time- averaged image (usually around fixed boundaries) and the pattern of fringes (and also the grating) is blurred in other parts of the image. Moreover, it is possible to reconstruct the modal eigenshape of the structural oscillations even if these oscillations are chaotic—if only the energy of oscillation is concentrated in one mode. Then moiré grating is visible not only around fixed boundaries, but also in the stationary regions defined by the eigenshape (though the time-averaged image is blurred in other regions). Finally, the decay rate of the sharpness of time-averaged moiré images can be used as an estimate of the largest Lyapunov exponent of chaotic oscil-

lations, especially when the same system is investigated at different forcing or other conditions.

V. CONCLUDING REMARKS

Time-average moiré constitutes a powerful experimental technique. Nevertheless, the solution of the inverse problem of reconstruction of the field of dynamic displacements (or strains) from patterns of time-averaged fringes in many cases requires skills and experience. Therefore, it is important to distinguish "wrong" measurement results caused by a malfunction of the optical system and physical reasons producing specific optical effects and caused by chaotic responses of nonlinear structures even under periodic forcing.

The analysis presented here of a vibrating disk performing chaotic oscillations and an appropriate one-dimensional system, provides insight into the physical reasons causing the pattern of time-averaged moiré fringes to disappear. An interpretation of the blurred time-averaged images is discussed. It is explained how to distinguish possible malfunctions of the optical system from effects caused by chaotic and nonperiodic oscillations. Moreover, it is shown what useful information about the eigenshape of oscillations one can extract from time-averaged moiré images if chaotic oscillations can be identified.

The effect of the disappearance of time-averaged fringes is demonstrated for reflection moiré. But the same effect would take place for time-average geometric moiré or time-average shadow moiré, since the physical relationships demonstrated for a one-dimensional system are valid for the above-mentioned variants of the moiré technique also.

[1] R. Neubecker and O. Jakoby, Phys. Rev. E **67**, 066221 (2003).

[2] A. S. Kobayashi, *Handbook on Experimental Mechanics*, 2nd ed. (SEM, Bethel, 1993).

[3] D. Post, B. Han, and P. Ifju, *High Sensitivity Moiré: Experimental Analysis for Mechanics and Materials* (Springer Verlag, Berlin, 1997).

[4] C. R. Schultheisz and W. G. Knauss, Opt. Lasers Eng. **20**, 283 (1994).

[5] P. Verleysen and J. Degrieck, Int. J. Impact Eng. **30**, 239 (2004).

[6] C. M. Liu and L. W. Chen, Ultramicroscopy **101**, 173 (2004).

[7] F. L. Dai and Z. Y. Wang, Opt. Lasers Eng. **31**, 191 (1999).

[8] X. Huimin, W. Guotao, D. Fulong, Z. Guangjun, L. Xingfu, and Z. Fangju, and X. Aiming, J. Mater. Process. Technol. **83**, 159 (1998).

[9] J. E. Field, S. M. Walley, W. G. Proud, H. T. Goldrein, and C. R. Siviour, Int. J. Impact Eng. **30**, 725 (2004).

[10] G. D'Alessandro, F. Papoff, E. Louvergneaux, and P. Glorieux, Phys. Rev. E **69**, 066212 (2004).

[11] M. Ragulskis, L. Ragulskis, and R. Maskeliunas, Exp. Tech. **28**, 27 (2004).

[12] M. Ragulskis, R. Maskeliunas, L. Ragulskis, and V. Turla, Opt. Lasers Eng. **43**, 951 (2005).

[13] R. C. Hilborn, *Chaos and Nonlinear Dynamics* (Oxford University Press, Norfolk, 2000).

[14] O. V. Gendelman, E. Gourdon, and C. H. Lamarque, J. Sound Vib. **294**, 651 (2006).

[15] J. Isohatala, K. N. Alekseev, L. T. Kurki, and P. Pietilainen, Phys. Rev. E **71**, 066206 (2005).

[16] P. Jacquod, Phys. Rev. E **72**, 056203 (2005).

[17] A. Ghosh and R. Ramaswamy, Phys. Rev. E **71**, 016224 (2005).

[18] A. H. Nayfeh, M. I. Younis, and E. M. Abdel-Rahman, Nonlinear Dyn. **41**, 211 (2005).

[19] G. Naganathan, S. Ramadhayani, and A. K. Bajaj, J. Vib. Control **9**, 95 (2003).

[20] T. Gross and U. Feudel, Phys. Rev. E **73**, 016205 (2006).

[21] P. Manzione and A. H. Nayfeh, J. Vib. Control **7**, 1013 (2001).

[22] M. Ragulskis, L. Saunoriene, and J. Ragulskiene, Opt. Lasers Eng. **44**, 1209 (2006).

[23] B. Blasius, Phys. Rev. E **72**, 066216 (2005).

[24] V. P. Namboodiri and S. Chaudhuri, Pattern Recogn. Lett. **28**, 311 (2007).